American Mineralogist, Volume 80, pages 1004–1019, 1995

One- and two-dimensional models of fluid flow and stable isotope exchange at an outcrop in the Adamello contact aureole, Southern Alps, Italy

Martha L. Gerdes, Lukas P. Baumgartner
Department of Geology and Geophysics, University of Wisconsin, Madison, Wisconsin 53706, U.S.A.
Mark Person
Department of Geology and Geophysics, University of Minnesota, Minneapolis, Minnesota 55455, U.S.A.
Douglas Rumble III
Geophysical Laboratory, Carnegie Institution of Washington, Washington, DC 20015, U.S.A.

Abstract

Localized depletion of ^{18}O and ^{13}C in a thin subhorizontal marble layer in the Adamello contact aureole, Southern Alps, Italy, resulted from fluid infiltration focused along a cross-cutting dike. Values of $\delta^{18}O$ and $\delta^{13}C$ in calcite from the 1 m long profile decrease systematically from sedimentary values of $\delta^{18}O = 22‰$ (SMOW) and $\delta^{13}C = 0‰$ (PDB) to $\delta^{18}O = 12.5‰$ and $\delta^{13}C \approx -7‰$ near the dike. The presence of clinozoisite and garnet in the 5–15 cm thick marble layers near the granodiorite dike indicates H_2O-rich fluid conditions ($X_{CO_2} \approx 0.01$).

The O and C isotope profiles were compared with one- and two-dimensional models of advective-dispersive isotope transport. Individually the isotope profiles fit one-dimensional transport models well. However one-dimensional models, using equilibrium fluid-rock exchange or a kinetic formulation, do not explain the relative locations or shapes of the two isotope-exchange profiles given the petrologic constraint of $X_{CO_2} \approx 0.01$ for the infiltrating fluid. Excellent agreement with the $\delta^{18}O$ and $\delta^{13}C$ data is obtained using a two-dimensional model that specifies (1) a high-permeability zone in marble near the dike that focuses fluid flow parallel to the dike and (2) a lower permeability zone in marble away from the dike where isotope exchange is dominated by molecular diffusion. The combined constraints imposed by phase equilibria and two isotope tracers allow two-dimensional fluid flow to be inferred from one-dimensional data. The results emphasize that isotope distributions resulting from multidimensional flow may fortuitously fit one-dimensional transport models if isotope tracers are considered independently. The use of multiple tracers coupled to fluid-composition constraints is therefore essential to discriminate between various transport models.

Introduction

Many recent studies of fluid flow during metamorphism have focused on models of one-dimensional stable isotope transport in homogeneous porous rock (e.g., Bickle and McKenzie, 1987; Baumgartner and Rumble, 1988; Lassey and Blattner, 1988; Blattner and Lassey, 1989; Bowman and Willett, 1991; Ferry and Dipple, 1992). These models show that one-dimensional fluid infiltration causes the development of smoothly varying isotope-exchange profiles, characterized by a transition from downstream rocks that preserve initial isotope values to upstream rocks that record the isotope composition of the infiltrating fluid. The application of one-dimensional models is justified for some simple geologic situations or as a first approximation if rock parameter information is lacking or boundary conditions are poorly understood. However, the interpretation of large-scale hydrothermal systems in terms of one-dimensional models is challenged by two-dimensional models of shallow cooling intrusions that indicate that fluid-flow patterns are transient and multidimensional (e.g., Cathles, 1977; Norton and Knight, 1977; Norton and Taylor, 1979; Taylor and Forester, 1979; Hanson, 1992; Gerdes et al., 1994). These two-dimensional models are consistent with several large-scale field studies, in which complex two- and three-dimensional isotope distributions were observed (Criss and Taylor, 1983; Criss and Fleck, 1990; Bowman et al., 1994; Roselle et al., 1994).

Given the complex flow patterns of large-scale hydrothermal systems, one-dimensional isotope transport models may be most appropriate for short transport distances. Indeed, one-dimensional models have reproduced isotope distributions at the meter scale (Baker et al., 1989; Ganor et al., 1989; Bickle and Baker, 1990; Cartwright and Valley, 1991). However, these models have typically evaluated the one-dimensional distribution of only one isotope tracer. The use of multiple tracers is preferable

0003–004X/94/0910–1004$02.00

because each provides an independent record of the hydrothermal event and thus improves constraints on transport models (Baumgartner and Rumble, 1988). Where two-dimensional data exist, there is strong evidence for channelized, multidimensional fluid flow even at a small scale (Baumgartner et al., 1989; Cartwright and Weaver, 1993; Cartwright, 1994). Since fluid-flow pathways can be quite complicated at all scales, the applicability of one-dimensional isotope transport models to any particular field site should be rigorously evaluated.

In this study we examine meter-scale ^{18}O and ^{13}C transport in a thin marble layer near a dike in the Adamello contact aureole, Southern Alps, Italy. Mineralogical and stable isotope changes in the marble layer occur systematically over < 1 m as the dike is approached. The changes in both $\delta^{18}O$ and $\delta^{13}C$ calcite values adjacent to the dike are similar to those predicted by one-dimensional transport models and therefore provide an excellent opportunity to test several one- and two-dimensional isotope transport models.

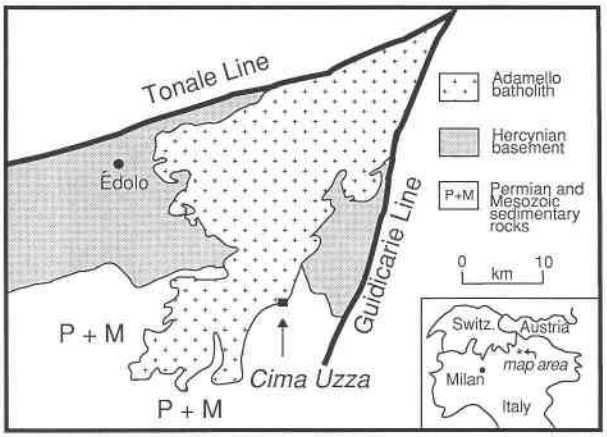

Fig. 1. Generalized map of the Adamello batholith, Southern Alps, Italy. The Cima Uzza field site is located at the southern margin of the batholith, where it intrudes previously unmetamorphosed Mesozoic sediments.

Regional geology

The outcrop described in this study is located on the southwest slope of Cima Uzza at the southern margin of the 700 km² Adamello batholith in the Southern Alps, northern Italy. The batholith was emplaced during the Tertiary into the shallow crust between the Tonale and Guidicarie Lines (Fig. 1). It consists dominantly of tonalite, but small cogenetic gabbro, diorite, and granodiorite stocks commonly occur at the massif margins (Callegari and Dal Piaz, 1973). The batholith intrudes Hercynian basement rocks in the north and Permian and Mesozoic sedimentary cover in the south (Fig. 1).

The Cima Uzza area exposes the southern contact of the Adamello tonalite and related mafic stocks with Triassic sediments, composed dominantly of dolomites, limestones, and marls (Fig. 2). The strata are generally flat-lying but dip increasingly downward toward the intrusion. Callegari (1962) and Bucher-Nurminen (1982) described the contact metamorphism of dolomites (< 1% silicates) at Cima Uzza. Bucher-Nurminen (1982) also mapped the forsterite isograd in the dolomites and determined calcite + dolomite temperatures (Fig. 2). Forsterite + chondrodite + spinel + calcite marbles, some with > 40% silicates, occur near the intrusion and in roof pendants, which Bucher-Nurminen (1982) interpreted to be products of Si and Al metasomatism.

The Calcare di Prezzo outcrop

The studied outcrop lies approximately 0.5 km south of the Adamello tonalite and is stratigraphically below the dolomite marbles described by Bucher-Nurminen (Fig. 2). The steep outcrop face exposes interlayered marble-marl layers of the Calcare di Prezzo Formation that are crosscut by a 0.5 m thick granodiorite dike (Fig. 3). The marl and marble layers are between 5 and 15 cm thick. The granodiorite dike (N40° E 82° NW) crosscuts these flat-lying layers (N34° E 30° SE) at a steep angle. A thin aplite dike, which was deformed and recrystallized during the Adamello contact metamorphism, also crosscuts the marble-marl layers. The focus of this study is a drill-core traverse across the thickest and most continuous marble layer adjacent to the granodiorite dike (Fig. 3). On the outcrop face this layer shows a slight discontinuity near the dike, but it is probably continuous in the third dimension (i.e., perpendicular to Fig. 3). The orientation of the steep outcrop surface relative to the orientation of the dike and sedimentary layering causes the minimum layer-parallel distances between drill-core samples and the dike to be less than the apparent distances as measured along the outcrop surface by a factor of two. In this study, the minimum layer-parallel distances to the dike, not the apparent outcrop face distances, are used.

Petrology

The marble layer shows significant mineralogical changes approaching the granodiorite dike. Away from the dike, the typical assemblage is calcite + plagioclase + tremolite + phlogopite + graphite + potassium feldspar + scapolite + diopside + sulfides + titanite (samples 637 and 638 in Table 1 and Fig. 3). Tremolite is absent in marbles closer to the dike. The typical assemblage for marbles at intermediate distances is calcite + diopside + phlogopite + feldspar + titanite + sulfides ± scapolite ± graphite (Fig. 4A, samples 906–914 and 630 in Table 1 and Fig. 3). Within approximately 40 cm of the dike, the mineral assemblage changes to calcite + garnet + diopside + clinozoisite + feldspar + titanite + sulfides ± scapolite ± phlogopite ± chlorite ± vesuvianite (samples 614 and 900–905 in Table 1 and Fig. 3). Garnet occurs only in this inner zone, where it forms poikilitic porphyroblasts (Fig. 4B). Garnet modal abundances, measured in the middle of the marble layer, are 13–31% within 25 cm of the contact and 1–8% from 25 to 40 cm (Table 1). Graphite occurs only in marbles > 64

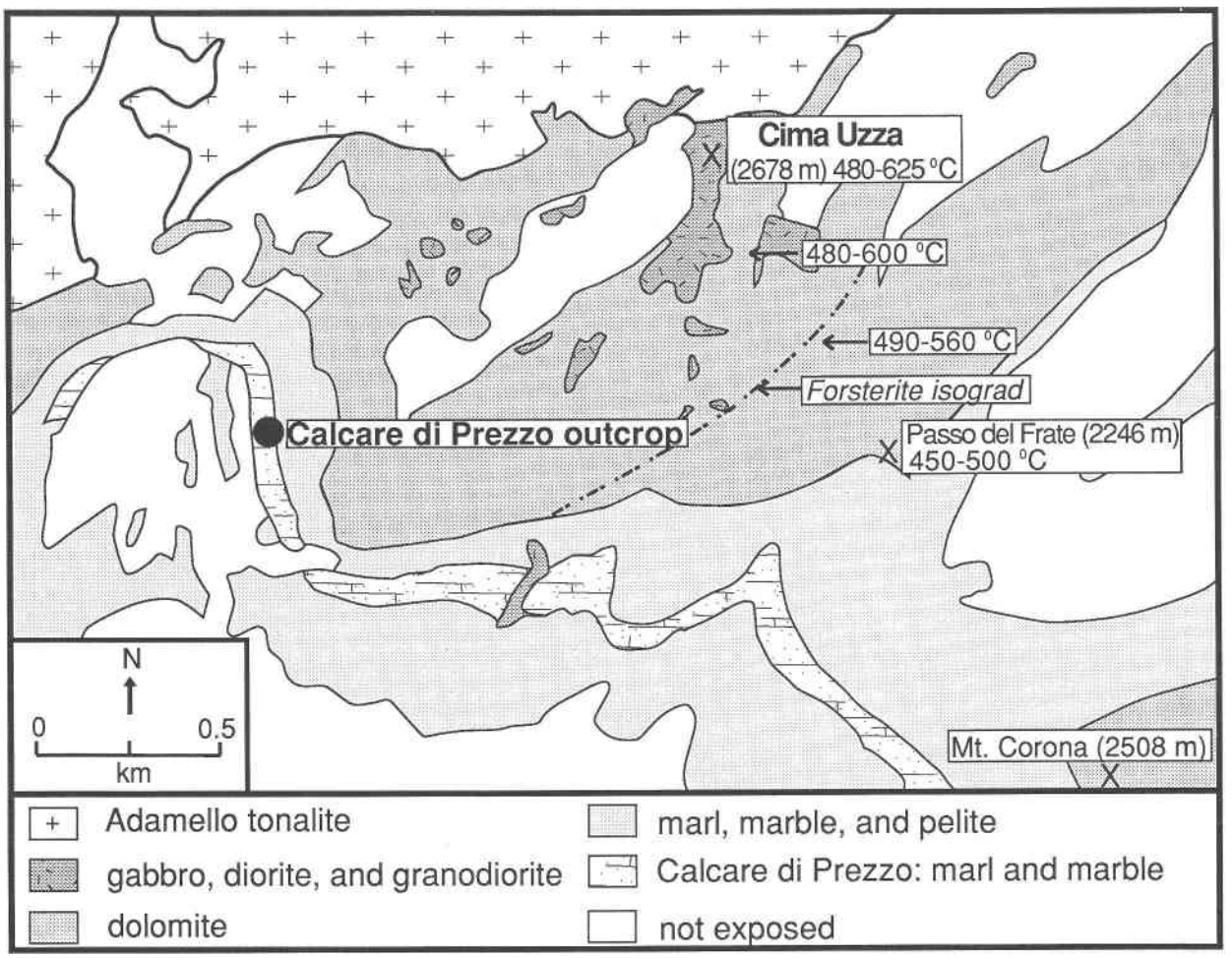

Fig. 2. Map of the Cima Uzza area, Southern Alps (after Brack, 1984). The Calcare di Prezzo outcrop is located south of the Adamello tonalite on the southwest slope of Cima Uzza. The forsterite isograd and calcite-dolomite solvus temperatures in dolomite marbles are from Bucher-Nurminen (1982).

cm from the contact. Calcite constitutes approximately 85% of most marble samples.

The mineral assemblage of the adjacent marl layers also changes systematically around the granodiorite dike. Farther than 44 cm from the dike, the marl assemblage is calcite + clinopyroxene + scapolite + plagioclase + biotite + sulfides ± chlorite ± titanite ± clinozoisite ± graphite. Calcite constitutes 10–20 modal% of these marls. Scapolite forms poikilitic porphyroblasts, which give the marl a mottled appearance (Fig. 4A). Graphite occurs only in marl samples >65 cm from the contact. Within 44 cm of the dike, the marl assemblage is clinopyroxene + garnet + clinozoisite + plagioclase + biotite + scapolite + sulfides ± vesuvianite ± titanite ± calcite ± chlorite ± potassium feldspar ± prehnite. Garnet and vesuvianite form large porphyroblasts with abundant inclusions of clinopyroxene and plagioclase. Calcite is less abundant within 44 cm of the dike and is absent in some samples.

Anhedral poikilitic garnets form a thin (0.2–1.0 cm) continuous rim between the marble and marl layers within 44 cm of the dike (Figs. 3 and 4B). These skarn interlayers consist almost entirely of garnet porphyroblasts, with some poikilitic vesuvianite porphyroblasts and minor clinozoisite, clinopyroxene, plagioclase, calcite, and biotite. The garnet rim is equally thick on the top and bottom of any given sedimentary layer.

Stable isotopes

O and C isotope data were collected from calcite in the marble layer at the Calcare di Prezzo outcrop. Powders for analysis were collected with a microdrill from drill-core slabs. They were collected >5 mm away from garnet porphyroblasts and from the contact with marl interlayers. The technique of McCrea (1950) and Sharma and Clayton (1965) was followed to extract CO_2 gas from the calcite powders. Isotopic analyses were made with a Nuclide gas-ratio mass spectrometer at the Geophysical Laboratory, Carnegie Institution of Washington, DC.

Both $\delta^{18}O$ and $\delta^{13}C$ values in the marble layer vary

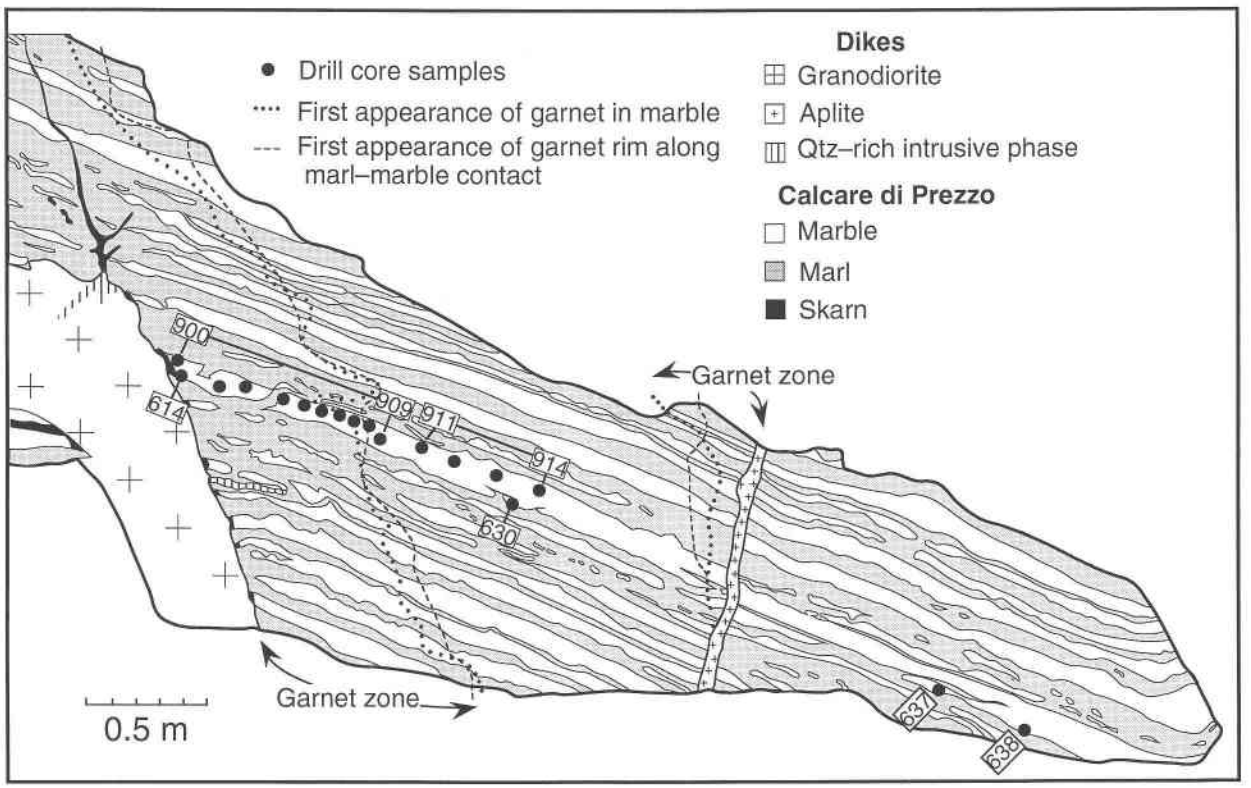

Fig. 3. Map of the Calcare di Prezzo outcrop at Cima Uzza, Southern Alps, Italy. Drill-core numbers correspond to samples described in Table 1. The outcrop surface is steep (S5° W 50° NW). The granodiorite dike (N40° E 82° NW) crosscuts the flat-lying sedimentary layers (N34° E 30° SE) at a steep angle.

systematically as a function of distance to the granodiorite dike (Table 1 and Fig. 5). Values of $\delta^{18}O$ at distances >50 cm from the dike are 21.0–22.5‰ (SMOW), typical values for Tethyan carbonates (Frisia-Bruni et al., 1989). These values decrease toward the dike to as low as 11.2‰. Values of $\delta^{13}C$ at distances >30 cm from the dike are −0.6 to +0.8‰ (PDB). Within 30 cm, $\delta^{13}C$ values are lower and heterogeneous, ranging from −8.0 to −4.8‰. The lower values of $\delta^{18}O$ and $\delta^{13}C$ near the dike suggest exchange with externally derived fluids.

Pressure-temperature-X_{CO_2} conditions

Although the age of the granodiorite dike at the Calcare di Prezzo outcrop has not been specifically constrained,

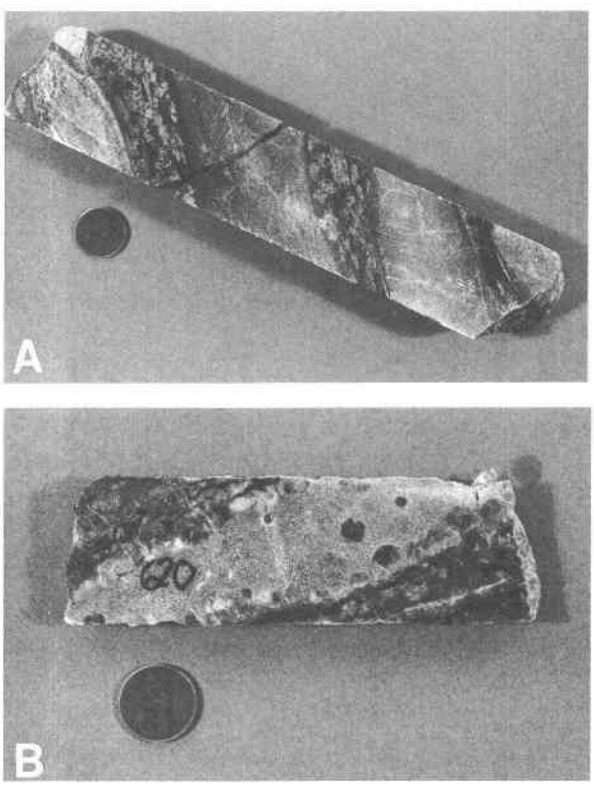

→

Fig. 4. (A) Photograph of marble and marl layers from drill core, showing the typical appearance of the Calcare di Prezzo unit >44 cm from the granodiorite dike. The four marble layers are lighter in color than the three marl interlayers. Porphyroblasts of scapolite give the marl layers a mottled appearance. (B) Photograph of marble and marl layers in drill core, showing the typical appearance of the Calcare di Prezzo unit within 40 cm of the granodiorite dike. A garnet rim separates the lighter colored marble from marl, and garnet porphyroblasts occur in both the marble and marl layers.

TABLE 1. Marble mineral assemblage and calcite stable isotope data for drill-core samples from the Calcare di Prezzo outcrop at Cima Uzza, Southern Alps, Italy

Sample	Distance to dike (cm)*	Mineral assemblage**	$\delta^{18}O$ (SMOW)	$\delta^{13}C$ (PDB)	Modal% garnet
614	2.5	cal, grt, di, czo, kfs, phl, op, ves	12.91	−7.69	13
			12.63	−7.60	
			12.57	−7.71	
			12.97	−7.95	
900†	3.5	cal, grt($Gr_{83}And_{15}Py_2$), di($Wo_{50}En_{32}Fs_{17}Jd_1$), phl, czo($Czo_{83}Ps_{17}$), chl, kfs, op, pl($An_2Ab_{98}$)	12.83	−6.16	13
			12.97	−5.86	
			12.74	−5.42	
			12.86	−5.14	
			13.02	−6.14	
			12.73	−4.81	
901	12.0	cal, grt, di, czo, fsp, op, ttn	11.24	−8.04	21
902	18.0	cal, di, grt, czo, op, phl, ttn, chl	13.35	−6.69	31
903	27.0	cal, grt, di, phl, scp, czo, fsp, op, ttn, chl	13.97	−5.54	5
904	31.0	cal, phl, di, grt, op, fsp, czo, scp, ttn	16.75	0.09	1
905	36.5	cal, di, phl, op, scp, fsp, grt, czo, ttn	16.75	−0.32	8
906	41.0	cal, di, phl, scp, op, fsp, ttn	19.43	−0.06	0
907	44.0	cal, di, phl, scp, fsp, op, ttn	20.20	0.37	0
908	47.5	cal, phl, di, fsp, scp, op, ttn	20.76	0.05	0
909	51.0	cal, phl, di, op, fsp, ttn	21.11	−0.64	0
			21.09	0.15	
911	58.5	cal, phl, di, fsp, op, ttn	21.25	−0.48	0
912	64.5	cal, fsp, phl, di, gr, scp, op, ttn	21.25	−0.48	0
913	74.5	cal, phl, fsp, di, gr, scp, ttn	22.25	0.58	0
630	77.0	cal, phl, fsp, gr, di, scp, ttn	22.38	0.83	0
			22.40	0.48	
			22.14	0.61	
914	83.5	cal, phl, di, gr, scp, ttn, op	22.50	0.26	0
637†	158.5	cal, pl($An_{39}Ab_{60}Or_1$), tr(Mg/Mg + Fe = 0.83), phl($Phl_{85}An_{15}$), gr, kfs($Or_{93}Ab_6An_1$), scp, di, op, ttn			0
638	190.5	cal, pl, phl, tr, gr, kfs, scp, op, di, ttn			0

* Distances are the minimum layer-parallel distance to the dike, not the distances measured directly along the outcrop face.

** Mineral abbreviations are as follows: cal = calcite, chl = chlorite, czo = clinozoisite, di = diopside, fsp = feldspar, gr = graphite, grt = garnet, kfs = potassium feldspar, op = opaque (mainly sulfides), phl = phlogopite, pl = plagioclase feldspar, scp = scapolite, tr = tremolite, ttn = titanite, and ves = vesuvianite. Feldspars not distinguished except in samples that were analyzed with an electron microprobe.

† The composition of selected mineral phases from samples 900 and 637 was determined with a Cameca SX-50 electron microprobe at the University of Wisconsin. These compositions, shown in parentheses, were used in calculating the phase diagram in Fig. 6.

field and petrologic observations indicate that the gabbro, tonalite, and granodiorite dikes at Cima Uzza are part of the same intrusive interval as the Adamello massif (Callegari, 1963). This field association and the mineral assemblages at the Calcare di Prezzo outcrop suggest that dike emplacement and resulting stable isotope shifts in the marble were synchronous with the main Adamello contact metamorphism. Lithostatic pressure during contact metamorphism at Cima Uzza is estimated at 1 kbar on the basis of phase equilibria and stratigraphic reconstructions (Schiavinato, 1946; Boriani and Origoni, 1982; McRae, 1983; Brack, 1984).

Metamorphic temperature and fluid composition in the clinozoisite + garnet marbles near the dike were estimated from the coexisting assemblage clinozoisite + calcite + garnet + diopside + plagioclase. The stability of this assemblage is restricted by three end-member reactions:

$$3 \text{ anorthite} + 1 \text{ calcite} + 1 H_2O = 2 \text{ clinozoisite} + 1 CO_2 \quad (1)$$

$$1 \text{ anorthite} + 1 \text{ quartz} + 2 \text{ calcite} = 1 \text{ grossular} + 2 CO_2 \quad (2)$$

$$26 \text{ calcite} + 15 \text{ diopside} + 20 \text{ clinozoisite} + 2 H_2O = 27 \text{ grossular} + 3 \text{ clinochlore} + 26 CO_2. \quad (3)$$

The PTX_{CO_2} conditions for these equilibria were calculated with the PERPLEX software package (Connolly, 1990) using the mineral compositions of sample 900 (Table 1) and the thermodynamic database and fluid equation of state of Holland and Powell (1990) (reaction curves 1a, 2, and 3 in Fig. 6). Grossular and diopside activities were calculated with the assumption of ideal mixing, clinozoisite activity was calculated from Bird and Helgeson (1980), and calcite, quartz, and chlorite were considered pure phases. An anorthite activity of 0.4 was used, even though this estimate is high for the measured plagioclase composition (An_2Ab_{98}). This value was used to provide a maximum X_{CO_2} position for reaction curve 1a (Fig. 6) and hence a maximum estimate of the X_{CO_2} composition of the infiltrating fluid.

In marble samples near the dike, the assemblage plagioclase + clinozoisite + calcite restricts T-X_{CO_2} conditions to fall along reaction curve 1a (Fig. 6). The absence of quartz requires temperatures above the intersection of reaction curves 1a and 2. The absence of coexisting chlo-

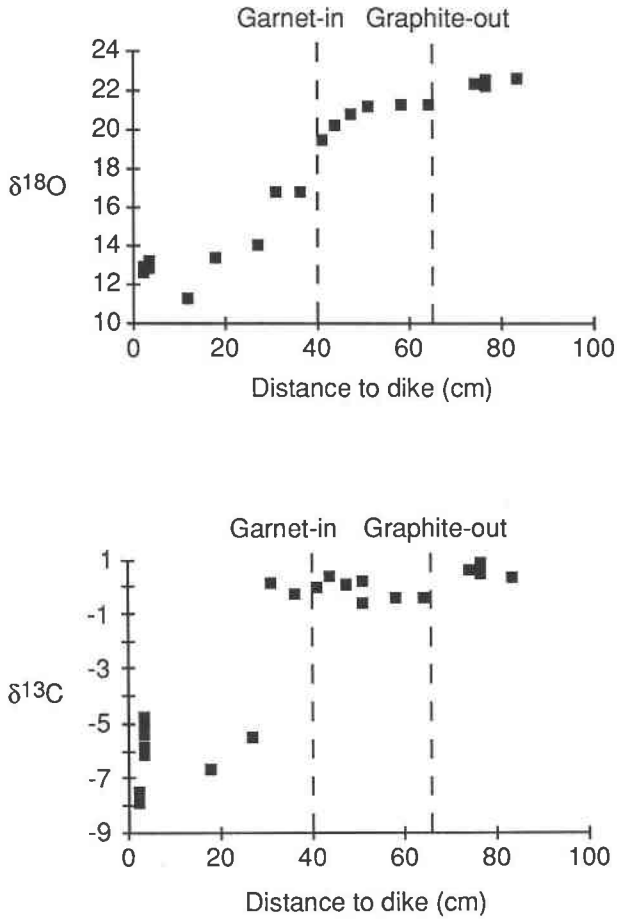

Fig. 5. Values of $\delta^{18}O$ (SMOW) and $\delta^{13}C$ (PBD) in calcite from a single marble layer at the Calcare di Prezzo outcrop, Cima Uzza, as a function of minimum layer-parallel distance to the granodiorite dike. Graphite is absent from marbles within 64 cm of the dike, and garnet occurs only within 40 cm.

rite and garnet requires temperatures below the intersection of reactions 1a and 3. The low-angle intersections of reaction curves 2 and 3 with reaction curve 1a causes the corresponding temperature limits (405–465 °C) to be imprecise, but these limits are consistent with calcite + dolomite temperatures from the overlying dolomites (Bucher-Nurminen, 1982). Even without precise temperature estimates, X_{CO_2} for the clinozoisite-garnet marbles is estimated at 0.01 because Reaction 1 is nearly vertical. Because closed-system mineral reactions in marble generate CO_2-rich fluids (e.g., Greenwood, 1975), the marbles near the dike must have reacted with externally derived, H_2O-rich fluid.

The tremolite marbles farthest from the dike contain the assemblage calcite + tremolite + diopside + potassium feldspar + plagioclase + phlogopite. This univariant assemblage apparently represents the end-member reaction:

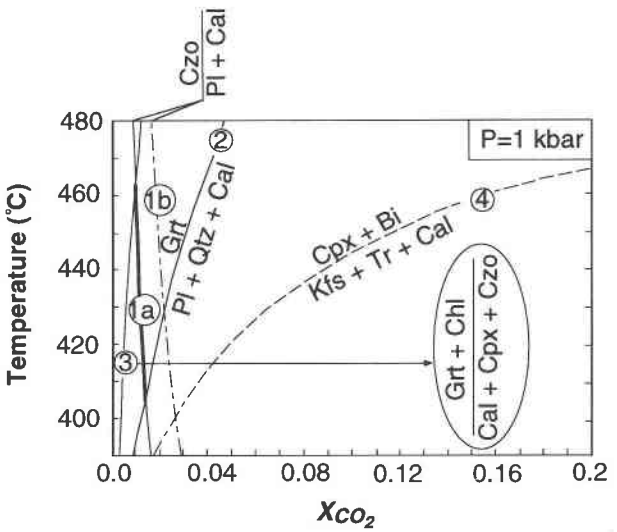

Fig. 6. Temperature-X_{CO_2} phase equilibria at $P = 1$ kbar governing metamorphic mineral assemblages in the marble layer at the Calcare di Prezzo outcrop, Cima Uzza. Numbers on the univariant curves correspond to reactions described in the text. Reactions 1a, 2, and 3 (solid lines) describe clinozoisite + garnet marbles near the dike and have been calculated using the mineral compositions in sample 900. Reactions 1b and 4 (dashed lines) describe tremolite marbles away from the dike and have been calculated using mineral compositions in sample 637.

1 potassium feldspar + 3 tremolite + 6 calcite
= 12 diopside + 1 phlogopite + 2 H_2O + 6 CO_2. (4)

The T-X_{CO_2} positions of Reactions 1 and 4, as corrected for mineral compositions in sample 637 (Table 1), are shown by curves 1b and 4 in Figure 6. Activities for tremolite, phlogopite, and potassium feldspar were calculated with the assumption of ideal solid solution. Anorthite activity was estimated at 0.8 from Carpenter and Ferry (1984), and calcite, clinopyroxene, and clinozoisite were considered pure phases. Reaction 4 reaches a temperature maximum at 495 °C and $X_{CO_2} \approx 0.75$. Because clinozoisite is absent, X_{CO_2} conditions must be more CO_2-rich than the intersection of curve 4 with curve 1b. Thus, T-X_{CO_2} conditions for sample 637 are constrained to fall along reaction curve 4, in the range $X_{CO_2} \geq 0.03$, 400 °C $\leq T \leq$ 495 °C. By assuming pure clinozoisite, curve 1b is positioned at a minimum X_{CO_2}; thus this lower X_{CO_2} limit for the tremolite marbles is a conservative estimate. These constraints suggest that the tremolite marbles were metamorphosed under at least slightly higher X_{CO_2} conditions than the clinozoisite marbles, but there is no petrologic evidence for a lateral temperature gradient away from the dike.

Isotope-exchange models

Stable isotope values and phase equilibria in the marbles indicate that infiltrating fluids were focused along the dike. The symmetrical garnet rim between the marble and marl layers argues against significant fluid infiltration

across sedimentary layers, which would result in asymmetrical rims. This constrains fluid flow to be approximately two-dimensional in the plane parallel to layering. Because there is no petrologic indication of a lateral thermal gradient across the marble layer, the following isotope transport models assume isothermal conditions. This assumption is reasonable because the long-term thermal effects from the Adamello batholith would likely override the local contributions from the granodiorite dike. Additional limits to the geometry of fluid flow are explored below by comparison of several one- and two-dimensional stable isotope-exchange models to the isotope data at the Calcare di Prezzo outcrop.

Isotope transport equations

The advective-dispersive transport of stable isotopes in a fluid moving through and reacting with porous rock has been derived in many previous studies (e.g., Lichtner, 1985; Bickle and McKenzie, 1987; Baumgartner and Rumble, 1988; Lassey and Blattner, 1988; Bowman and Willett, 1991; Dipple and Ferry, 1992; Bowman et al., 1994), and only a short discussion will be presented here. The isotope transport equations assume single-phase fluid flow through a fully saturated, incompressible rock matrix. If isotope exchange between fluid (fl) and rock (rx) is fast relative to fluid velocity, the approximation of instantaneous local equilibrium can be made. With this assumption, the O isotope transport equation is

$$\left[1 + \frac{K_D(1-\phi)\nu^O_{rx}\hat{V}_{fl}}{\phi\nu^O_{fl}\hat{V}_{rx}}\right]\frac{\partial(R^{18O}_{fl})}{\partial t} = \nabla\cdot\tilde{D}\nabla R^{18O}_{fl} - \bar{v}\cdot\nabla R^{18O}_{fl} \quad (5)$$

where K_D is the equilibrium rock-fluid fractionation, ϕ is porosity, ν^O the O stoichiometry coefficient in fluid or rock, $\hat{V}$ the molar fluid or rock volume, $\bar{v}$ the average linear fluid velocity vector, R^{18O} is mol^{18}O/mol^{16}O, t is time, and $\tilde{D}$ is the dispersion tensor combining contributions from both molecular diffusion and mechanical dispersion. The parenthetical expression that multiplies the time derivative in Equation 5 is known as the retardation factor (R_D) because it quantifies the distance that the midpoint of an isotope front lags behind the actual front of the infiltrating fluid. Because the retardation factor reflects the relative tracer abundance in the fluid and rock, different isotope tracers have different retardation factors, causing the development of spatially separate isotope fronts (Baumgartner and Rumble, 1988).

The dimensionless ratio of advective to dispersive mass transport, known as the Peclet number, is commonly used to describe one-dimensional solutions to Equation 5:

$$N_{Pe} = \frac{\bar{v}L}{D} \quad (6)$$

where L is an arbitrary unit length. A large Peclet number is characteristic of isotope transport when fluid velocity is high relative to dispersion, causing a relatively sharp exchange front. A low Peclet number characterizes isotope transport dominated by dispersion, which creates a more diffuse isotope-exchange zone. In this study, L is taken to be 100 cm, the length of the isotope profiles across the Calcare di Prezzo outcrop.

If isotope-exchange rates are too slow for the assumption of instantaneous local equilibrium, a kinetic formulation for fluid-rock exchange is required. Following Cole et al. (1983), Lassey and Blattner (1988), Bowman and Willett (1991), and Bowman et al. (1994), this study uses a first-order kinetic rate law:

$$\frac{\partial(R^{18O}_{rx})}{\partial t} = \kappa(K_D R^{18O}_{fl} - R^{18O}_{rx}) \quad (7)$$

where κ is the rate of the isotope-exchange reaction. With this formulation the O isotope transport equation is

$$\frac{\partial(R^{18O}_{fl})}{\partial t} + \left[\frac{(1-\phi)\nu^O_{rx}\hat{V}_{fl}}{\phi\nu^O_{fl}\hat{V}_{rx}}\right]\kappa(K_D R^{18O}_{fl} - R^{18O}_{rx}) = \nabla\cdot\tilde{D}\nabla R^{18O}_{fl} - \bar{v}\cdot\nabla R^{18O}_{fl}. \quad (8)$$

The Damköhler-I number is a dimensionless parameter that describes one-dimensional solutions to Equation 8 (Boucher and Alves, 1959; Lassey and Blattner, 1988):

$$N_D = \frac{\kappa L}{\bar{v}}. \quad (9)$$

A large Damköhler-I number means that isotope exchange is fast compared with advective transport and may effectively act as an equilibrium-exchange process. At lower Damköhler-I numbers, exchange rates are slower relative to transport, resulting in diffuse isotope-exchange fronts.

In this study, the dispersion tensor, $\tilde{D}$, in Equations 5 and 8 includes contributions from both molecular diffusion in the fluid phase and from mechanical dispersion resulting from physical mixing of fluid at the pore scale. Molecular diffusion is a scalar property of the fluid. Mechanical dispersion increases with fluid velocity and is described by a symmetric second-order tensor. This study uses a common formulation for mechanical dispersion parallel to fluid flow (Bear, 1972):

$$D_L = \alpha_L\cdot\bar{v} \quad (10)$$

where α_L is longitudinal dispersivity. Mechanical dispersion perpendicular to fluid flow is given by

$$D_T = \alpha_T\cdot\bar{v} \quad (11)$$

where α_T is transverse dispersivity. We assume that longitudinal and transverse dispersivity values are constant in a given lithologic unit.

These mathematical formulations are the basis for comparison of three isotope-exchange models with the O and C isotope data from the Calcare di Prezzo outcrop.

Model 1: One-dimensional fluid flow with equilibrium isotope exchange

The first model considers equilibrium stable isotope exchange during one-dimensional fluid infiltration parallel to the marble layer and perpendicular to the dike

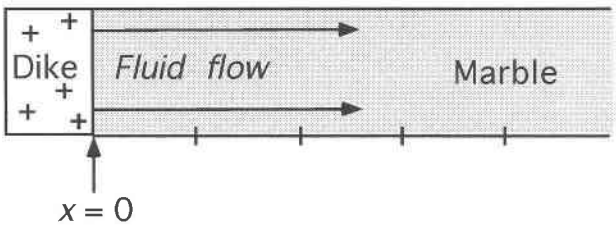

Fig. 7. Geologic model for one-dimensional equilibrium and kinetic isotope exchange at the Calcare di Prezzo outcrop. Fluid infiltrates perpendicular to the dike along the marble layers, starting at the dike contact.

(Fig. 7 and Eq. 5). The model assumes that $\delta^{18}O$ and $\delta^{13}C$ values in the marble were initially homogeneous, and that at $t \geq 0$ a fluid of a different but constant composition infiltrated the marble starting at the dike contact ($x = 0$). With these initial and boundary conditions, Equation 5 can be solved analytically for each isotope tracer (e.g., Ogata and Banks, 1961). Its four independent variables are as follows: (1) vt/R_D, which approximates the transport distance from the dike to the midpoint of the isotope front; (2) Dt/R_D, which describes the dispersive spreading around the midpoint of the isotope front; (3) $\delta^{18}O_i$ or $\delta^{13}C_i$, the initial marble composition before infiltration begins; and (4) $\delta^{18}O_0$ or $\delta^{13}C_0$, the composition of the marble at the dike contact in equilibrium with the infiltrating fluid.

The O and C isotope data from the Calcare di Prezzo outcrop have been independently fit to the one-dimensional equilibrium isotope transport model using a Marquardt-type, nonlinear, least-squares fit procedure (Bevington, 1969). The best-fit solution to the $\delta^{18}O$ data is shown in Figure 8A. This solution yields values of 34.1 ± 1.0 cm for the distance to the isotope front (vt/R_D), 63.5 ± 14.5 cm² for Dt/R_D, 22.1 ± 0.2‰ for $\delta^{18}O_i$, and 12.7 ± 0.2‰ for $\delta^{18}O_0$. The resulting Peclet number is 53.7 ± 1.7. This solution fits the O isotope data well, as indicated by a low χ^2 per degree of freedom (χ^2/F) value of 1.2.

The best-fit solution to the C isotope data is shown in Figure 9A. Values of $\delta^{13}C$ are scattered within 30 cm of the dike, resulting in a higher χ^2/F of 3.1. The solution yields values of 28.0 ± 1.8 cm for the distance to the isotope front (vt/R_D), 0.5 ± 1.2 cm² for Dt/R_D, 0.1 ± 0.1‰ for $\delta^{13}C_i$, and −6.6 ± 0.1‰ for $\delta^{13}C_0$. The Peclet number is 5600 ± 180.

Even though a one-dimensional equilibrium-exchange model independently fits the O and C data well (Figs. 8A and 9A), two serious discrepancies arise when comparing the fits. The first is the large difference in best-fit Peclet numbers. The Peclet number from the C profile is 100 times larger than the O Peclet number. For similar diffusion coefficients for O and C, the Peclet numbers calculated from the two isotope profiles should be the same if the one-dimensional equilibrium isotope-exchange model were applicable. The high C Peclet number is reflected in the steeper shape of the $\delta^{13}C$ exchange profile

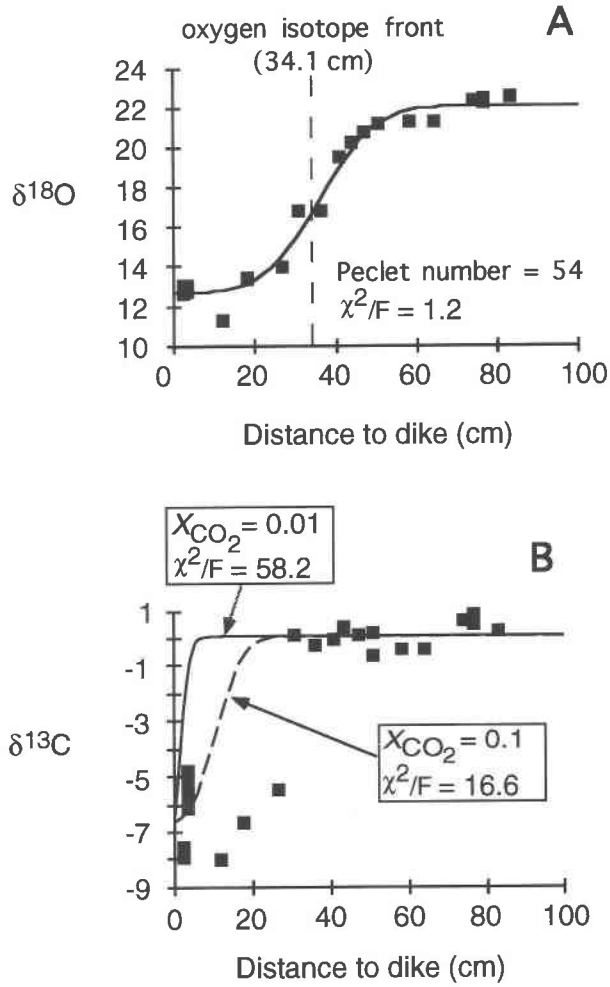

Fig. 8. (**A**) The best-fit curve to the $\delta^{18}O$ data using a one-dimensional equilibrium isotope-exchange model. (**B**) Two predicted $\delta^{13}C$ profiles, at X_{CO_2} = 0.01 and 0.1, using a one-dimensional equilibrium-exchange model and the best-fit Peclet number from the $\delta^{18}O$ data (above). The specification of fluid composition constrains the predicted location of the C front relative to the observed location of the O front, determined by the best-fit solution (above) to be at 34.1 cm.

(Fig. 9A), in contrast to the more diffuse $\delta^{18}O$ profile (Fig. 8A).

The second discrepancy between the independent fits to the O and C isotope profiles is the relative displacement of the isotope fronts away from the dike (vt/R_D). Phase equilibria indicate an X_{CO_2} of 0.01 in the clinozoisite + garnet marbles. This constraint can be used to calculate retardation factors for C and O (Eq. 5). Since C is much less abundant than O in the H_2O-rich binary H_2O-CO_2 infiltrating fluid, it has a larger retardation factor, and the isotope front would not propagate as far into the marble layer. For a pure calcite rock and a fluid composition of X_{CO_2} = 0.01, the C front would lag approximately 34 times behind the O front. However, the actual C front, located at 28 cm from the dike, is only 1.2 times

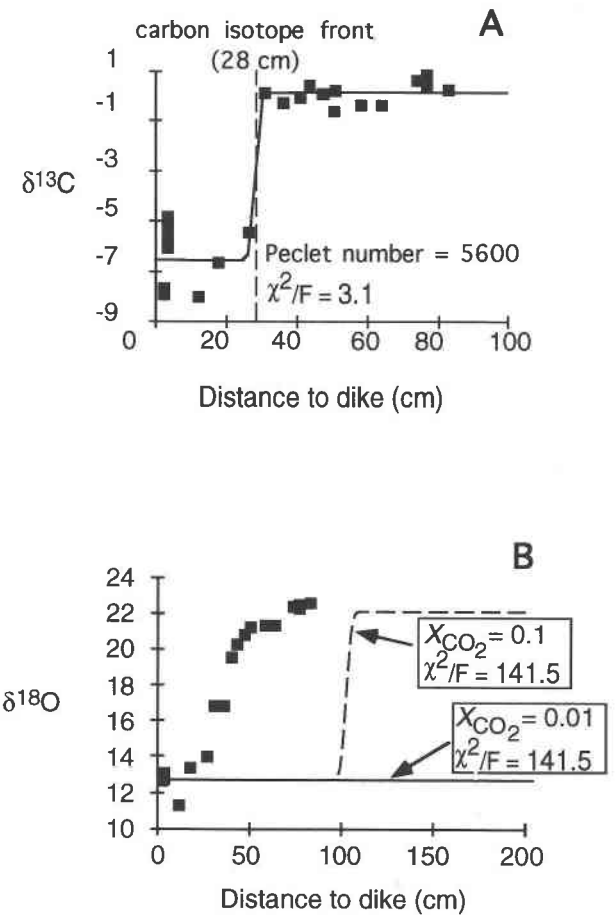

Fig. 9. (**A**) The best-fit curve to the $\delta^{13}C$ data using a one-dimensional equilibrium isotope-exchange model. (**B**) Two predicted $\delta^{18}O$ profiles, at X_{CO_2} = 0.01 and 0.1, using a one-dimensional equilibrium-exchange model and the best-fit Peclet number from $\delta^{13}C$ data (above). The specification of fluid composition constrains the predicted location of the O front relative to the observed location of the C front, determined by the best-fit solution (above) to be at 28 cm.

behind the O front, positioned at 34 cm. The observed lag implies an infiltrating fluid with $X_{CO_2} \approx 0.4$, which is considerably more CO_2-rich than petrologic estimates.

The discrepancies between the O and C isotope profiles are illustrated in Figures 8B and 9B. Figure 8B shows the predicted position of the C profile relative to the observed position of the O isotope front (Fig. 8A) if $X_{CO_2} = 0.01$, using the O best-fit Peclet number (54). The profile is displaced only a few centimeters into the marble layer and is a very poor match to the observed C data (χ^2/F = 58.2). Even at $X_{CO_2} = 0.1$, an order of magnitude higher than petrologic estimates, the predicted C profile is closer to the dike than the actual C data ($\chi^2/F = 16.6$). Similarly, Figure 9B shows two predicted O isotope profiles relative to the observed position of the C isotope front, for X_{CO_2} = 0.01 and $X_{CO_2} = 0.1$, using the C best-fit Peclet number (5600). The predicted O fronts are at 104 cm for X_{CO_2} = 0.1 and 944 cm for $X_{CO_2} = 0.01$ (not shown fully in figure). Both calculated profiles are extremely poor matches to the O isotope data. Values of χ^2/F are 141.5 for the two predicted O profiles because the profiles are identical over the distances for which isotope data exist. A one-dimensional equilibrium isotope-exchange model produces good individual fits to the O and C profiles (Figs. 8A and 9A), but it is not consistent if the two isotope profiles were formed simultaneously in an H_2O-rich flow system (Figs. 8B and 9B).

Model 2: One-dimensional fluid flow with kinetic isotope exchange

To help explain the discrepancies in the one-dimensional equilibrium-exchange model, the second model explores the possibility that kinetically limited isotope exchange, not dispersion, accounts for the curvature in the $\delta^{18}O$ profile. The fluid-infiltration model is the same as that for the one-dimensional equilibrium-exchange case (Fig. 7). However, in this second model, isotope exchange between fluid and rock is described by a first-order kinetic rate law (Eq. 7) with tracer-dependent reaction rates.

Because the C isotope data show a sharp (~7‰) gradient over only a few centimeters (Fig. 9A), it is assumed for this second model that the C profile was not significantly influenced by mechanical dispersion, molecular diffusion, or kinetically limited isotope exchange, all of which would make the profile more diffuse. The C isotope profile can therefore be approximated in a one-dimensional flow regime by advective transport with an instantaneous fluid-rock exchange rate. This approximation produces a sharp C front, positioned 28 cm from the dike as determined previously by the one-dimensional equilibrium-exchange model (Fig. 9A).

Because dispersion and diffusion should be virtually the same for O as for C, these effects can be assumed negligible in the formation of the O profile as well. The diffuse O isotope profile can therefore result only from O having a slower exchange rate than C. Equation 8 can be solved analytically in one dimension for advection and rate-limited isotope exchange (Goldstein, 1953; Lassey, 1982; Lassey and Blattner, 1988). Using the analytical solution and a nonlinear least-squares fitting procedure, the best fit to the O isotope data (Fig. 10, dashed line) was obtained. The best-fit solution estimates the distance to the O isotope front, vt/R_D, at 35.4 ± 0.04 cm and a Damköhler-I number of 20.2 ± 5.3. The solution fits the O isotope data well (χ^2/F = 1.1).

As with the previous model, however, this best fit is not consistent with petrologic constraints on X_{CO_2} and with the observed position of the C front. For instance, even at an X_{CO_2} value of 0.1, which is ten times larger than the petrologic estimate, the O isotope front should be 104 cm from the dike. This is almost three times farther than is predicted by the best-fit solution. Figure 10 shows the predicted O isotope profiles for an O isotope front at 104 cm but with different Damköhler-I numbers

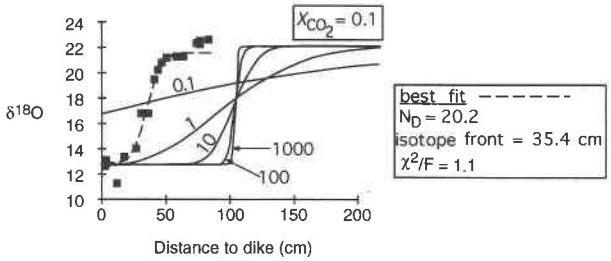

Fig. 10. The best-fit solution to the $\delta^{18}O$ profile at the Calcare di Prezzo outcrop using a one-dimensional kinetic isotope-exchange model (dashed line). In addition, the predicted O isotope profiles, all based on X_{CO_2} = 0.1, using several Damköhler-I numbers are shown (solid lines). The specified fluid composition of X_{CO_2} = 0.1 constrains the predicted location of the O front relative to the observed C front (at 28 cm, Fig. 9A).

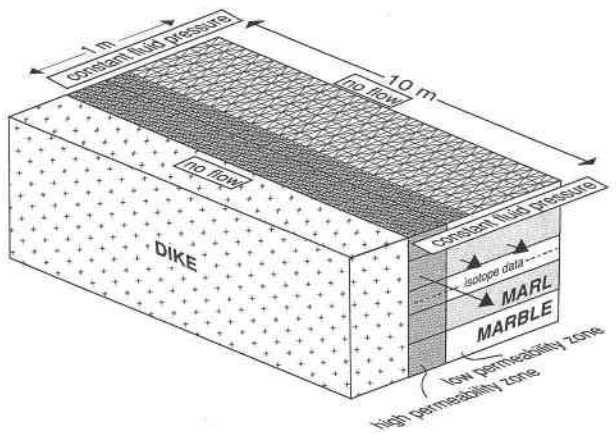

Fig. 11. Geologic model of two-dimensional equilibrium isotope exchange at the Calcare di Prezzo outcrop. Fluid infiltrates parallel to the granodiorite dike and to the marble-marl layers. It is focused through a high-permeability zone within 25 cm of the dike. This width corresponds to the marble rich in hydrothermal garnet. Marble >25 cm from the dike is considered to be three orders of magnitude less permeable. The finite-element mesh used in the C isotope transport simulation and the boundary conditions are superimposed.

(solid lines). At higher Damköhler-I numbers (N_D = 10, 100, and 1000 in Fig. 10), the predicted O isotope fronts are farther from the dike than the observed front. At lower Damköhler-I numbers (N_D = 0.1 and 1 in Fig. 10), the predicted exchange fronts are significantly more diffuse than the observed data. For the X_{CO_2} value of 0.01 estimated from petrology, the predicted isotope-exchange front is 944 cm from the dike, resulting in an even poorer fit to the data. Therefore, a one-dimensional kinetic exchange model cannot reproduce the observed $\delta^{18}O$ values.

For this kinetic exchange model to be plausible, a mechanism that produces slower exchange for O than C is required. Isotope exchange controlled by volume diffusion is the only reasonable mechanism to produce different exchange rates for different isotopes. However, diffusion experiments indicate that C diffusion rates in calcite are several orders of magnitude slower than O at metamorphic temperatures (Kronenberg et al., 1984). These experiments suggest that if rate-limited exchange had been important at the Calcare di Prezzo outcrop, the C profile would be more diffuse than the O profile. Because this prediction is opposite that observed in the C and O profiles, the diffusion experiments substantiate the difficulties of the one-dimensional kinetic isotope-exchange model.

Model 3: Two-dimensional fluid flow with equilibrium isotope exchange

Because neither one-dimensional model explains both the C and O data, a two-dimensional equilibrium isotope-exchange model was tested (Eq. 5). The geologic model for the two-dimensional problem is illustrated in Figure 11. In this model, fluid flow was assumed to be parallel to the dike and to sedimentary layering. The presence of >10 modal% hydrothermal garnet (Table 1) within 25 cm of the dike was thought to indicate a high-permeability zone that channelized Si- and Al-bearing H_2O-rich fluid. Farther away from the dike, where garnet is minor or absent, a lower-permeability zone was assumed.

Estimation of model variables. Fluid composition is estimated to have been X_{CO_2} = 0.01 from phase equilibria. Fluid density is assumed constant over time and throughout the outcrop. The initial model $\delta^{18}O$ value of the marble is 22.2‰, and the $\delta^{18}O$ value of the marble in equilibrium with the infiltrating fluid is 12.5‰, as suggested by the data in Figure 5. The initial $\delta^{13}C$ value is 0.0‰, and the $\delta^{13}C$ value of the marble in equilibrium with the infiltrating fluid is −9.0‰. The marble is modeled as pure calcite.

Other variables needed to solve the two-dimensional problem are fluid velocity, permeability, porosity, molecular diffusion, and longitudinal and transverse dispersivities in the high- and low-permeability marble zones. Estimates for these variables are not independently available for the Calcare di Prezzo rocks themselves. Instead they were taken from published values and were adjusted within reasonable limits to optimize the fit to the paired O and C profiles (Table 2). The range over which these variables can reasonably be adjusted is often several orders of magnitude. For instance, rates of molecular diffusion in the fluid phase in porous media depend on the dominant transport mechanism. Depending on the permeability structure, diffusion could be dominated by either grain-boundary diffusion or by diffusion through a free fluid (e.g., Joesten, 1991). The range of possible molecular diffusion rates is therefore quite large, ranging from 10^{-17} to 10^{-7} m²/s (Nagy and Giletti, 1986; Farver and Yund, 1991; Walton, 1960; Ildefonse and Gabis, 1976). A diffusion rate of 5×10^{-10} m²/s was used in the two-dimensional model.

The importance of mechanical dispersion has been recognized in several metamorphic flow systems (Bowman

TABLE 2. Fluid, rock, and transport parameters used in two-dimensional model compared with published estimates

	Model values for high-permeability zone	Model values for low-permeability zone	Published estimates	References*
Porosity	10^{-3}	10^{-4}	10^{-6}–10^{-3}	2, 8, 10, 13
Permeability (m^2)	10^{-15}	10^{-18}	10^{-23}–10^{-12}	1, 2, 3, 5, 6, 8, 13, 14
Fluid velocity (m/s)	3×10^{-10}	3×10^{-13}	2×10^{-14}–3×10^{-9}	1, 2, 4, 5, 8, 9, 13
Molecular diffusion through fluid (m^2/s)	5×10^{-10}	5×10^{-10}	10^{-17}–10^{-7}	7, 12, 15, 16
Longitudinal dispersivity (m)	10^{-1}	10^{-1}	10^{-2}–10^{2}	11
Transverse dispersivity (m)	10^{-2}	10^{-2}	$\sim 10^{-3}$–10^{1}	11
Initial rock $\delta^{18}O$ (‰)	22.2	22.2		
Initial rock $\delta^{13}C$ (‰)	0.0	0.0		
X_{CO_2} of infiltrating fluid	0.01	0.01		
Rock $\delta^{18}O$ in equilibrium with infiltrating fluid (‰)	12.5	12.5		
Rock $\delta^{13}C$ in equilibrium with infiltrating fluid (‰)	−9.0	−9.0		

* 1 = Baumgartner and Ferry (1991), 2 = Bickle and Baker (1990), 3 = Brace (1980), 4 = Cartwright (1994), 5 = Cartwright and Weaver (1993), 6 = Clauser (1992), 7 = Farver and Yund (1991), 8 = Ferry and Dipple (1991), 9 = Ferry and Dipple (1992), 10 = Ganor et al. (1989), 11 = Gelhar et al. (1992), 12 = Ildefonse and Gabis (1976), 13 = Léger and Ferry (1993), 14 = Manning et al. (1993), 15 = Nagy and Giletti (1986), 16 = Walton (1960).

et al., 1994; Cartwright, 1994), but there are no laboratory or field estimates of mechanical dispersion under metamorphic conditions. Many researchers of metamorphic fluid flow previously assumed that molecular diffusion was the major contribution to the dispersion tensor (Bickle and McKenzie, 1987; Bickle and Baker, 1990; Bickle, 1992; Cartwright, 1994). In one-dimensional transport models, omitting the mechanical dispersion tensor from transport formulations is relatively inconsequential because the tensor reduces to a scalar in one dimension, transverse dispersion is not considered, and dimensionless solutions are obtained without isolating the specific contributions of mechanical dispersion. However, in two-dimensional models and where a range of flow velocities are inferred to exist, velocity-dependent mechanical dispersion can have a critical effect on modeling predictions. In the hydrogeology literature, values of longitudinal dispersivity for transport scales of 1–100 m vary from 10^{-2} to 10^{2} m (Gelhar et al., 1992). Hydrogeologic studies find that transverse dispersivities are often approximately one order of magnitude smaller than longitudinal dispersivity in a given aquifer (Gelhar et al., 1992). For lack of direct estimates, this study assumes that longitudinal dispersivities in contact metamorphic flow systems are similar to hydrogeologic dispersivities, and that transverse dispersivity is one order of magnitude smaller than longitudinal dispersivity. The model described below uses a longitudinal dispersivity of 10^{-1} m and a transverse dispersivity of 10^{-2} m. With this assumption, mechanical dispersion rates are higher than molecular diffusion in the high-velocity zone and are lower than molecular diffusion in the low-velocity zone.

Finite-element solution. Because there is no analytical solution to this two-dimensional problem, the finite-element method (e.g., Reddy, 1984; Huyakorn and Pinder, 1983), applied over triangular elements using linear basis functions, was used to calibrate the model. O and C isotope transport were solved separately using different mesh designs, but variable estimates were identical in each set of simulations. O isotope transport was represented using a grid composed of 241 columns and 23 rows, simulating a 60 m flow path along the dike and a 1 m exchange zone perpendicular to it. The tight grid spacing reduces the computational error from numerical dispersion, which can be large near steep isotope gradients.

The finite-element mesh used for the C transport simulations is superimposed on the model design in Figure 11. C transport was modeled with a 51-column, 23-row grid, simulating a 10 m flow path along the dike and a 1 m exchange zone perpendicular to it. The flow path was shorter for the C isotope models than for the O isotopic models because the C exchange front migrates more slowly through the marble, and hence a 10 m flow path is adequate to represent the region of isotope exchange.

In the simulations, fluid with a constant isotopic composition was introduced at one end of the domain and allowed to flow through the marble layer parallel to the dike. Constant fluid-pressure values were specified for the input and output boundaries, and the resulting fluid-velocity field was constant throughout the transient simulation. No-flow boundaries were specified for the sides. Fluid velocities, constrained by Darcy's Law, were three times higher in the high-permeability zone near the dike than in the low-permeability zone.

Two-dimensional simulation results. Many paired O and C isotope models were tested with different variable estimates. The results of one of these models are shown in Figures 12 and 13. Figure 12 shows contours of $\delta^{18}O$ and $\delta^{13}C$ in the marble layer at two time steps in the simulation (10000 and 20000 yr). Because fluid velocities are three times faster in the high-permeability zone, the O and C fronts propagate more quickly through this zone than in the low-permeability zone. Slow fluid velocities in the low-permeability marble cause mechanical disper-

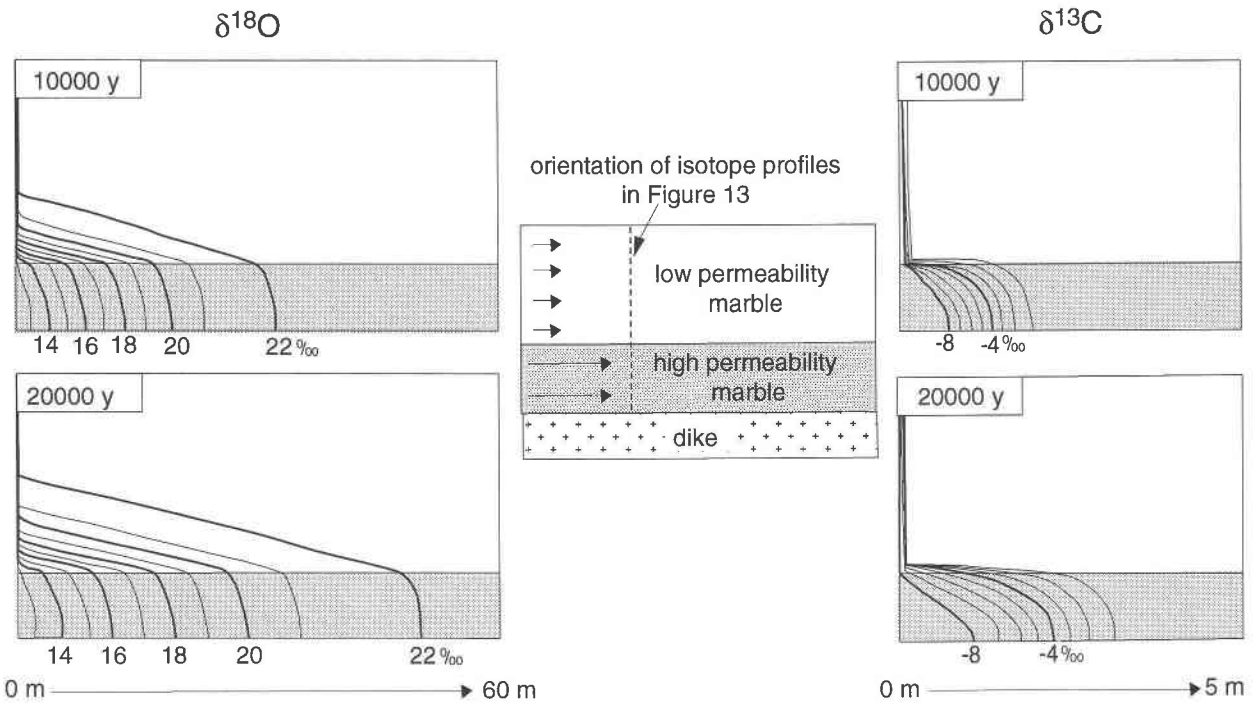

Fig. 12. Contours of $\delta^{18}O$ (left) and $\delta^{13}C$ (right) in the marble layer at two time steps in the calibrated two-dimensional simulation. The contour interval for both $\delta^{18}O$ and $\delta^{13}C$ is 1‰. A schematic illustration of the two-dimensional isotope-exchange model (center) shows fluid infiltrating parallel to the dike from the left boundary to the right. The resulting isotope fronts propagate more rapidly through the high-permeability marble (shaded) than through the low-permeability marble (unshaded). The migration rate of the C isotope front through the marble is slower than that of the O isotope front, as constrained by the specified fluid composition of $X_{CO_2} = 0.01$ (note scale differences). Isotope distributions at 20000 yr are the basis for the one-dimensional profiles shown in Fig. 13.

sion to be small (Eqs. 10 and 11), so that molecular diffusion accounts for most of the isotope transport in this region.

To compare the model results with the isotope data, one-dimensional profiles perpendicular to the dike at different distances along the flow path were taken from the two-dimensional model (Fig. 13). Figure 13A shows predicted $\delta^{18}O$ profiles after 20000 yr at 12 positions along the flow path. In any given profile, the solution shows relatively low and homogeneous $\delta^{18}O$ values in the high-permeability zone and a diffusion-dominated zone extending from the 25 cm interface into the low-permeability zone. The four profiles showing the most O isotope exchange in Figure 13A are all good fits to the observed O isotope data. Figure 13B shows the predicted $\delta^{13}C$ values at five different positions along the flow path. These five profiles correspond to the five most altered profiles in Figure 13A. Beyond the fourth profile, no noticeable C isotope alteration has occurred even though $\delta^{18}O$ values continue to show alteration for much greater distances. The low abundance of C in the fluid also means that there is little diffusion of low $\delta^{13}C$ fluids into the low-permeability zone, causing a sharp $\delta^{13}C$ gradient between the high- and low-permeability marbles. The profile showing the most ^{13}C exchange (thick line in Fig. 13B) is a good fit to the C data. This profile corresponds to the profile showing the most ^{18}O exchange (thick line in Fig. 13A). The excellent match between these predicted profiles and the O and C data therefore verifies that a two-dimensional model can reproduce the isotope profiles using geologically reasonable parameter estimates.

Discussion

Justification and limitations of the two-dimensional model

A two-dimensional equilibrium-exchange model provides a better fit to both the C and O data than the one-dimensional models. The inference that fluid infiltrates parallel to the dike is consistent with other studies that show the preferential channeling of metamorphic fluids along discrete structural discontinuities or within certain lithologies (e.g., Hover-Granath et al., 1983; Nabelek et al., 1984; Ferry, 1987; Baumgartner et al., 1989; Bickle and Baker, 1990; Baumgartner and Ferry, 1991; Cartwright, 1994). Both before and after crystallization, dikes

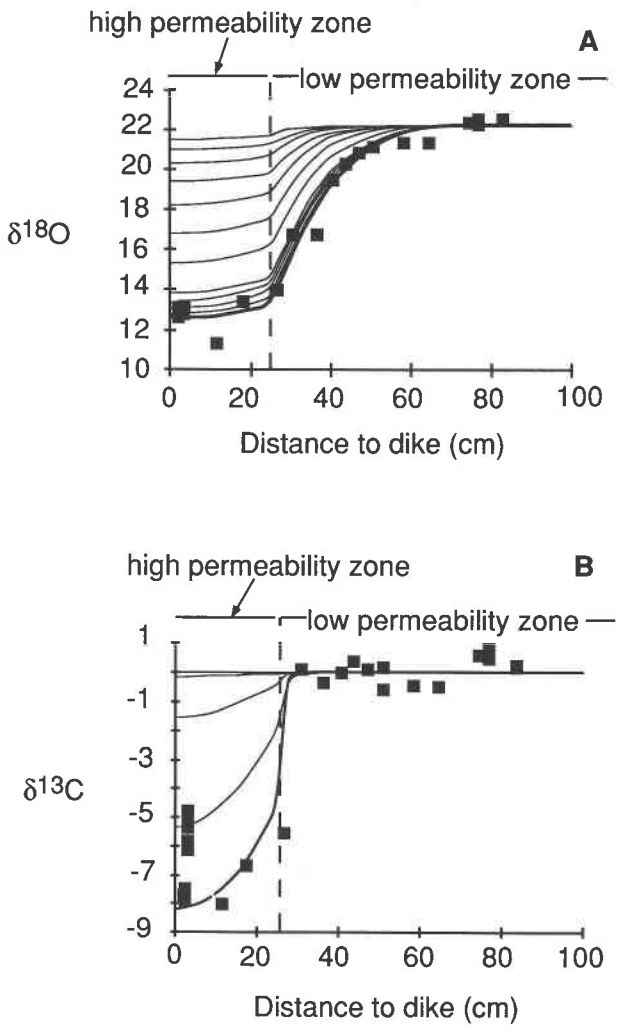

Fig. 13. (**A**) Comparison of the $\delta^{18}O$ data to 12 predicted profiles taken perpendicular to the dike at different distances along the 60 m flow path at 20000 yr in the calibrated two-dimensional simulation (Fig. 12). (**B**) Comparison of the $\delta^{13}C$ data to five predicted profiles taken perpendicular to the dike at different distances along the 10 m flow path at 20000 yr in the calibrated two-dimensional simulation (Fig. 12). The five predicted C profiles correspond to the five most altered O isotope profiles in **A**.

are probably a common type of small-scale fluid barrier. Before complete crystallization, magmas are believed to be impermeable (Furlong et al., 1991). Even after crystallization, dikes remain less permeable than surrounding sedimentary rocks, unless fractured, because they are less likely to undergo porosity-generating metamorphic reactions. At the Calcare di Prezzo outcrop, the lack of hydrothermal mineral alteration in the granodiorite dike is evidence of low permeability. In contrast, a garnet-rich skarn marks the contact between the dike and adjacent marble layers (Fig. 3), showing that this contact was a high-permeability pathway.

Despite the general advantages of the two-dimensional model, the specific solution shown in Figures 12 and 13 is not unique. This is because few of the parameters needed to solve the two-dimensional problem for this particular outcrop can be determined independently. Within reasonable ranges, several combinations of variable estimates result in an equally good fit to the data. Because the two-dimensional model predicts different isotope profiles in the same marble layer at different distances along the dike (Fig. 13), additional model limits would be available from sampling elsewhere along the same dike. However, limited outcrop exposure at the Calcare di Prezzo outcrop does not allow the same layer to be sampled anywhere else, and the two-dimensional model presented here cannot be further refined without these two-dimensional data. Because the data come from only one distance along the dike, the large-scale direction of fluid flow within the contact aureole cannot be inferred. Indeed, given the heterogeneity of hydrothermal systems, it seems likely that this flow model cannot be extrapolated significantly beyond the scale of observation. It is possible to determine only that locally a significant component of the fluid flow was subhorizontal and parallel to both the dike and marble layer. Although the two-dimensional model suggests only meter-scale isotope exchange, this does not necessarily indicate that the dike itself was the fluid source. Given the abundant veining in many hydrothermal systems, it seems possible that the hydrothermal fluid that infiltrated the Calcare di Prezzo outcrop originated in the main Adamello massif or smaller mafic stocks and was channelized for hundreds of meters with minimal isotopic interaction.

The assumption in the two-dimensional model that all flow is parallel to the dike is a simplification of the actual flow patterns. Some fluid may have leaked laterally into the sedimentary layers, as is indicated by the garnet rims along the marble-marl interfaces (Figs. 3 and 4B). The assumption that porosity and permeability are constant over time is also an approximation. The infiltration of fluids along the dike contact drove metamorphic reactions, which in turn would have locally increased permeability in the marble. The correlation between garnet growth and stable isotope alteration within 25 cm of the dike is indicative of this kind of reaction-enhanced permeability. The clinozoisite + garnet marbles near the dike probably had heterogeneous permeabilities at any given time. However, the uncertainties and simplifications inherent in the two-dimensional model do not negate the conclusion that such a model is a good representation of the Calcare di Prezzo outcrop, whereas a one-dimensional model cannot reproduce the isotopic observations.

Heterogeneity in C data

A notable characteristic of the isotope data from the Calcare di Prezzo outcrop is the heterogeneity of $\delta^{13}C$ values near the dike. Values of $\delta^{13}C$ within 25 cm of the dike are highly variable even within single drill-core samples (−8.0 to −4.8‰). This heterogeneity is attributed to

three possible causes. First, variations in permeability are expected to produce more variation in $\delta^{13}C$ values than in $\delta^{18}O$ values. This is because variable amounts of isotope exchange resulting from variations in permeability are most evident at the isotope front, where the steepest isotope gradients occur. At the Calcare di Prezzo outcrop, the C front moving parallel to the dike has not moved as far as the O front (Fig. 12), so the sampled traverse is necessarily much closer to the C front than the O front. Because the steep isotope gradients around the C front (Fig. 13B) are much closer to the sampled area, the $\delta^{13}C$ values are expected to preserve evidence of permeability variations more noticeably than the $\delta^{18}O$ values. A second explanation for the heterogeneous C data is that the C isotope composition of the H_2O-rich infiltrating fluid could have been modified by mixing with small amounts of a different fluid. The abundance of O in the fluid would make it less susceptible to $\delta^{18}O$ shifts from small amounts of mixing. Finally, local variability in the amount of CO_2-producing metamorphic reactions could cause variable depletion of ^{13}C owing to Rayleigh distillation. Because the amount of calcite in the garnet + clinozoisite rocks near the contact is not significantly less than in the tremolite marbles away from the contact, this distillation effect is unlikely to exceed 1 or 2 per mill (Valley, 1986). Because graphite disappears before changes in $\delta^{13}C$ occur (Fig. 5), reaction of graphite does not appear to be related to the $\delta^{13}C$ heterogeneity.

Conclusions

Because isotope-alteration patterns are the cumulative result of fluid interaction, few of the physical and geochemical parameters governing isotope exchange can be uniquely determined. Many large- and small-scale field sites that show isotopic evidence for fluid interaction are therefore poorly suited for isotope transport modeling. Isotope transport modeling at the Calcare di Prezzo outcrop is possible only because flow-geometry constraints and petrologic restrictions on fluid composition can be coupled with data from multiple tracers. Considered individually, the one-dimensional $\delta^{18}O$ and $\delta^{13}C$ profiles from this outcrop conform well to equilibrium one-dimensional transport models. Without the restrictions on fluid composition provided by phase equilibria, the isotope-exchange profiles in the marble layer could be easily mistaken as advective-dispersive isotope fronts resulting from one-dimensional infiltration perpendicular to the dike. Instead, the one-dimensional models cannot reproduce the observed isotope-alteration patterns of both tracers unless the fluid composition was much more CO_2-rich than phase equilibria allows. A two-dimensional model consistent with phase equilibria is successful in reproducing the $\delta^{18}O$ and $\delta^{13}C$ profiles at the outcrop, showing that fluid infiltrated parallel to the dike and was focused along a high-permeability marble zone adjacent to the contact. Yardley and Lloyd (1995) speculate that many apparent metasomatic fronts in hydrothermally altered metamorphic rocks actually represent the sides of higher-permeability fluid-flow channels. The results of this study are consistent with their predictions, showing that the $\delta^{18}O$ and $\delta^{13}C$ exchange fronts at the Calcare di Prezzo outcrop are more reasonably taken to be sides resulting from multidimensional flow.

Acknowledgments

We thank K.R. Lassey for providing the K-function algorithms (Lassey, 1982), D. Slawinski for providing UNIX system technical support, and G.T. Roselle for assistance in the University of Wisconsin microprobe lab. IBM Corporation donated a RISC 6000 workstation, on which most of the simulations were performed. Additional support for this research came from an NSF graduate fellowship to M.L.G., NSF grant EAR-9316504 and National Young Investigator award EAR-9257160 to L.P.B., and NSF grants EAR-9304873 and EAR-9405807 to M.P. This paper was improved by reviews from J. Bowman, M. Kohn, S. Olsen, G. Roselle, and E. Young.

References cited

Baker, J., Bickle, M.J., Buick, I.S., Holland, T.J.B., and Matthews, A. (1989) Isotopic and petrological evidence for the infiltration of water-rich fluids during the Miocene M2 metamorphism on Naxos, Greece. Geochimica et Cosmochimica Acta, 53, 2037–2050.

Baumgartner, L.P., and Ferry, J.M. (1991) A model for coupled fluid flow and mixed volatile mineral reactions with applications to regional metamorphism. Contributions to Mineralogy and Petrology, 106, 273–285.

Baumgartner, L.P., and Rumble, D. (1988) Transport of stable isotopes: I. Development of a kinetic continuum theory for stable isotope transport. Contributions to Mineralogy and Petrology, 98, 417–430.

Baumgartner, L.P., Gieré, R., Trommsdorff, V., and Ulmer, P. (1989) Field guide for the Southern Adamello. In V. Trommsdorff, P. Ulmer, R. Gieré, L.P. Baumgartner, Eds., Guidebook for the excursion to the Central Alps, Bergell and Adamello, p. 91–115. Consiglio Nazionale delle Ricerche, Sienna, Italy.

Bear, J. (1972) Dynamics of fluids in porous media, 764 p. Dover, New York.

Bevington, P.R. (1969) Data reduction and error analysis for the physical sciences, 336 p. McGraw-Hill, New York.

Bickle, M.J. (1992) Transport mechanisms by fluid-flow in metamorphic rocks: Oxygen and strontium decoupling in the Trois Seigneurs Massif: A consequence of kinetic dispersion? American Journal of Science, 292, 289–316.

Bickle, M.J., and Baker, J. (1990) Advective-diffusive transport of isotopic fronts: An example from Naxos, Greece. Earth and Planetary Science Letters, 97, 78–93.

Bickle, M.J., and McKenzie, D. (1987) The transport of heat and matter by fluids during metamorphism. Contributions to Mineralogy and Petrology, 95, 384–392.

Bird, D.K., and Helgeson, H.C. (1980) Chemical interaction of aqueous solutions with epidote-feldspar mineral assemblages in geologic systems: I. Thermodynamic analysis of phase relations in the system CaO-FeO-Fe_2O_3-Al_2O_3-SiO_2-H_2O-CO_2. American Journal of Science, 280, 907–941.

Blattner, P., and Lassey, K.R. (1989) Stable isotope exchange fronts, Damköhler numbers, and fluid-rock ratios. Chemical Geology, 78, 381–392.

Boriani, A., and Origoni, E.G. (1982) Heat transfer in the thermo-metamorphic aureole of the northeastern sector of Mt. Adamello (Trento-Italy). Rendiconti della Società Italiana di Mineralogia e Petrologia, 38, 1351–1360.

Boucher, D.F., and Alves, G.E. (1959) Dimensionless numbers for fluid mechanics heat transfer, mass transfer, and chemical reaction. Chemical Engineering Progress, 55, 55–64.

Bowman, J.R., and Willett, S.D. (1991) Spatial patterns of oxygen isotope exchange during one-dimensional fluid infiltration. Geophysical Research Letters, 18, 971–974.

Bowman, J.R., Willett, S.D., and Cook, S.J. (1994) Oxygen isotopic trans-

port and exchange during fluid flow: One-dimensional models and applications. American Journal of Science, 294, 1–55.

Brace, W.F. (1980) Permeability of crystalline rocks and argillaceous rocks. International Journal of Rock Mechanics and Mineral Science, 17, 241–251.

Brack, P. (1984) Geologie der Intrusiva und Rahmengesteine des Suedwest-Adamello (Nord-Italien), 235 p. Ph.D. thesis, Eidgenossichen Technische Hochschule, Zurich, Switzerland.

Bucher-Nurminen, K. (1982) On the mechanism of contact aureole formation in dolomitic country rock by the Adamello intrusion (northern Italy). American Mineralogist, 67, 1101–1117.

Callegari, E. (1962) La Cima Uzza (Adamello Sud-Orientale): I. Studio petrografico e petrogenetico delle formazioni metamorfiche di contatto. Memorie degli Istituti di Geologia e Mineralogia dell'Universita di Padova, 23, 116 p.

——— (1963) La Cima Uzza (Adamello Sud-Orientale): II. Studio petrographico e petrogenetico della massa femica. Memorie degli Istituti di Geologia e Mineralogia dell'Universita di Padova, 24, 127 p.

Callegari, E., and Dal Piaz, G.B. (1973) Field relationships between the main igneous masses of the Adamello Intrusive Massif (N. Italy). Memorie degli Istituti di Geologia e Mineralogia dell'Universita di Padova, 29, 1–39.

Carpenter, M.A., and Ferry, J.M. (1984) Constraints on the thermodynamic mixing properties of plagioclase feldspars. Contributions to Mineralogy and Petrology, 87, 138–148.

Cartwright, I. (1994) The two-dimensional pattern of metamorphic fluid flow at Mary Kathleen, Australia: Fluid focusing, transverse dispersion, and implications for modeling fluid flow. American Mineralogist, 79, 526–535.

Cartwright, I., and Valley, J.W. (1991) Steep oxygen isotope-gradients at marble-metagranite contacts in the northwest Adirondack Mountains, New York, USA: Products of fluid-hosted diffusion. Earth and Planetary Science Letters, 107, 148–163.

Cartwright, I., and Weaver, T.R. (1993) Metamorphic fluid flow at Stephen Cross Quarry, Quebec: Stable isotopic and petrologic data. Contributions to Mineralogy and Petrology, 113, 533–544.

Cathles, L.M. (1977) An analysis of the cooling of intrusives by groundwater convection which includes boiling. Economic Geology, 72, 804–826.

Clauser, C. (1992) Permeability of crystalline rocks. Eos, 73(21), 233–240.

Cole, D.R., Ohmoto, H., and Lasaga, A.C. (1983) Isotopic exchange in mineral-fluid systems: I. Theoretical evaluation of oxygen isotope exchange accompanying surface reactions and diffusion. Geochimica et Cosmochimica Acta, 47, 1681–1693.

Connolly, J.A.D. (1990) Multivariable phase diagrams: An algorithm based on generalized thermodynamics. American Journal of Science, 290, 666–718.

Criss, R.E., and Fleck, R.J. (1990) Oxygen isotope map of the giant metamorphic-hydrothermal system around the northern part of the Idaho batholith, U.S.A. Applied Geochemistry, 5, 641–655.

Criss, R.E., and Taylor, H.P. (1983) An $^{18}O/^{16}O$ and D/H study of Tertiary hydrothermal systems in the southern half of the Idaho batholith. Geological Society of America Bulletin, 94, 640–663.

Dipple, G.M., and Ferry, J.M. (1992) Fluid flow and stable isotopic alteration in rocks at elevated temperatures with applications to metamorphism. Geochimica et Cosmochimica Acta, 56, 3539–3550.

Farver, J.R., and Yund, R.A. (1991) Measurement of oxygen grain boundary diffusion in natural, fine-grained quartz aggregates. Geochimica et Cosmochimica Acta, 55, 1597–1608.

Ferry, J.M. (1987) Metamorphic hydrology at 13-km depth and 400–550 °C. American Mineralogist, 72, 39–58.

Ferry, J.M., and Dipple, G.M. (1991) Fluid flow, mineral reactions, and metasomatism. Geology, 19, 211–214.

——— (1992) Models for coupled fluid flow, mineral reaction, and isotopic alteration during contact metamorphism: The Notch Peak aureole, Utah. American Mineralogist, 77, 577–591.

Frisia-Bruni, S., Jadoul, F., and Weissert, H. (1989) Evinosponges in the Triassic Esino Limestone (Southern Alps): Documentation of early lithification and late diagenesis overprint. Sedimentology, 36, 685–699.

Furlong, K.P., Hanson, R.B., and Bowers, J.R. (1991) Modeling thermal regimes. In Mineralogical Society of America Reviews in Mineralogy, 26, 437–506.

Ganor, J., Matthews, A., and Paldor, N. (1989) Constraints on effective diffusivity during oxygen isotope exchange at a marble-schist contact, Sifnos (Cyclades), Greece. Earth and Planetary Science Letters, 94, 208–216.

Gelhar, L.W., Welty, C., and Rehfeldt, K.R. (1992) A critical review of data on field-scale dispersion in aquifers. Water Resources Research, 18, 1955–1974.

Gerdes, M.L., Baumgartner, L.P., and Person, M.A. (1994) A geostatistical approach to modeling the effect of heterogeneous permeabilities during contact metamorphism. Geological Society of America Abstracts with Programs, 26, 42.

Goldstein, S. (1953) On the mathematics of exchange processes in fixed columns, I. Proceedings of the Royal Society, Series, 219A, 151–171.

Greenwood, H.J. (1975) Buffering of pore fluids by metamorphic reactions. American Journal of Science, 275, 573–593.

Hanson, R.B. (1992) Effects of fluid production on fluid flow during regional and contact metamorphism. Journal of Metamorphic Geology, 10, 87–97.

Holland, T.J.B., and Powell, R. (1990) An enlarged and updated internally consistent thermodynamic database with uncertainties and correlations: The system K_2O-Na_2O-CaO-MgO-MnO-FeO-Fe_2O_3-Al_2O_3-TiO_2-SiO_2-C-H_2-O_2. Journal of Metamorphic Geology, 8, 89–124.

Hover-Granath, V.C., Papike, J.J., and Labotka, T.C. (1983) The Notch Peak contact metamorphic aureole, Utah: Petrology of the Big Horse member of the Orr Formation. Geological Society of America Bulletin, 94, 889–906.

Huyakorn, P.S., and Pinder, G.F. (1983) Computational methods in subsurface flow, 473 p. Academic, New York.

Ildefonse, J.P., and Gabis, V. (1976) Experimental study of silica diffusion during metasomatic reactions in the presence of water at 550 °C and 1,000 bars. Geochimica et Cosmochimica Acta, 40, 297–303.

Joesten, R. (1991) Kinetics of coarsening and diffusion-controlled mineral growth. In Mineralogical Society of America Reviews in Mineralogy, 26, 507–582.

Kronenberg, A.K., Yund, R.A., and Giletti, B.J. (1984) Carbon and oxygen diffusion in calcite: Effects of Mn content and P_{H_2O}. Physics and Chemistry of Minerals, 11, 101–112.

Lassey, K.R. (1982) On the computation of certain integrals containing the modified Bessel function $I_0(\zeta)$. Mathematics of Computation, 39, 625–637.

Lassey, K.R., and Blattner, P. (1988) Kinetically controlled oxygen isotope exchange between fluid and rock in one-dimensional advective flow. Geochimica et Cosmochimica Acta, 52, 2169–2175.

Léger, A., and Ferry, J.M. (1993) Fluid infiltration and regional metamorphism of the Waits River Formation, north-east Vermont, USA. Journal of Metamorphic Geology, 11, 3–30.

Lichtner, P.C. (1985) Continuum model for simultaneous chemical reactions and mass transport in hydrothermal systems. Geochimica et Cosmochimica Acta, 49, 779–800.

Manning, C.E., Ingebritsen, S.E., and Bird, D.K. (1993) Missing mineral zones in contact metamorphosed basalts. American Journal of Science, 293, 894–938.

McCrea, J.M. (1950) On the isotope chemistry of carbonates and a paleotemperature scale. Journal of Chemical Physics, 18, 849–857.

McRae, T. (1983) The Adamello complex: Aspects of its emplacement and uplift. Ph.D. thesis, University of Cambridge, Cambridge, U.K.

Nabelek, P.I. Labotka, T.C., O'Neil, J.R., and Papike, J.J. (1984) Contrasting fluid/rock interaction between the Notch Peak granitic intrusion and argillites and limestones in western Utah: Evidence from stable isotopes and phase assemblages. Contributions to Mineralogy and Petrology, 85, 25–34.

Nagy, K.L., and Giletti, B.J. (1986) Grain boundary diffusion of oxygen in a micro-perthitic feldspar. Geochimica et Cosmochimica Acta, 50, 1151–1158.

Norton, D., and Knight, J. (1977) Transport phenomena in hydrothermal systems: Cooling plutons. American Journal of Science, 277, 937–981.

Norton, D., and Taylor, H.P., Jr. (1979) Quantitative simulation of the

hydrothermal systems of crystallizing magmas on the basis of transport theory and oxygen isotope data: An analysis of the Skaergaard intrusion. Journal of Petrology, 20, 421–486.

Ogata, A., and Banks, R.B. (1961) A solution of the partial differential equation of longitudinal dispersion in porous media. U.S. Geological Survey Professional Paper, 411-A.

Reddy, J.N. (1984) An introduction to the finite element method, 495 p. McGraw-Hill, New York.

Roselle, G.T., Baumgartner, L.P., and Valley, J.W. (1994) Fluid flow in the Ubehebe Peak contact aureole, Last Chance Mts., California. Geological Society of America Abstracts with Programs, 26, 225.

Schiavinato, G. (1946) Il giacimento e wollastonite ed altri minerali di contatto presso Alpe Bazena. Memorie degli Istituti di Geologia e Mineralogia dell'Universita di Padova, 15, 1–61.

Sharma, T., and Clayton, R.N. (1965) Measurement of $^{18}O/^{16}O$ ratios of total oxygen of carbonates. Geochimica et Cosmochimica Acta, 29, 1347–1353.

Taylor, H.P., Jr., and Forester, R.W. (1979) An oxygen and hydrogen study of the Skaergaard intrusion and its country rocks: A description of a 55-m.y.-old fossil hydrothermal system. Journal of Petrology, 20, 355–419.

Valley, J.W. (1986) Stable isotope geochemistry of metamorphic rocks. In Mineralogical Society of America Reviews in Mineralogy, 16, 445–489.

Walton, M. (1960) Molecular diffusion rates in supercritical water vapor estimated from viscosity data. American Journal of Science, 258, 385–401.

Yardley, B.W.D., and Lloyd, G.E. (1995) Why metasomatic fronts are really metasomatic sides. Geology, 23, 53–56.

Manuscript received November 14, 1994
Manuscript accepted June 7, 1995